Supporting Information for

In-situ Observation of Heterogeneous Charge Distribution at the Electrode Unraveling the Mechanism for the Electric-field Enhanced Electrochemical Activity

Rong Jin,[a] Yuchen Huang,[a] Lei Cheng,[b] Hongyan Lu,[a] Dechen Jiang,*[a] and Hongyuan Chen[a]

Table of Contents

Theoretical derivation of the ionic concentrations in diffuse layer and the ionic current.

When a voltage is applied to the electrode surface, the ion concentrations in diffuse layer can be calculated according to Boltzmann distribution:[S1-3]

$$c_{-} = c_{-0} e^{\frac{e\varphi}{kT}}$$
$$c_{+} = c_{+0} e^{-\frac{e\varphi}{kT}} \qquad \text{(eq. S1)}$$

where φ is the potential at the distance x from the electrode, c_- and c_+ are the concentrations of negative and positive ion at a potential of φ, k is Boltzmann constant, and T is thermodynamic temperature. $e\varphi$ is the potential energy that refers to the energy for the moving of the charge from infinity to φ.

In our work, 20 mM H_2SO_4 solution was chosen as electrolyte that could be ionized into H^+ and HSO_4^- ions in the first stage. With a secondary ionization constant of 0.012, the concentrations of $[H^+]$, $[HSO_4^-]$ and $[SO_4^{2-}]$ were estimated to be 20.24, 19.76 and 0.24 mM, respectively.[S2]

From equation S1, c_- and c_+ can be described when the relationship between φ and x is determined. The expression of φ can be derived from the Poisson equation in electromagnetism:[S1a]

$$\varphi = \frac{2kT}{e} \ln\left(\frac{2}{1 - \frac{e^{\frac{e\varphi_0}{2kT}} - 1}{e^{\frac{e\varphi_0}{2kT}} + 1} e^{-\kappa x}} - 1 \right) \qquad \text{(eq. S2)}$$

where φ_0 is the voltage applied to the electrode and x is the distance from the electrode surface among the diffuse layer. κ is the reciprocal of the thickness of the electric double layer, which can be obtained by the following relationship:[S1c]

$$\kappa = \left(\frac{2c_0 N_A e^2}{\varepsilon kT} \right)^{\frac{1}{2}} \qquad \text{(eq. S3)}$$

where N_A is the Avogadro constant, ε is the solution dielectric constant, and κ can be determined from the fixed solution concentration at room temperature (298 K). ε_r for 20 mM H_2SO_4 is considered as 81.5 and κ is 2.48E8 m^{-1}. Thus, the Debye length ($1/\kappa$) is about 4 nm.

However, the Debye length from our simulation result is ~ 14 nm (Figure 2A). This error might be ascribed to the simulation using eq. S3, which works well under a small potential. In our study, a potential of -0.3 or -0.5 V were not tiny enough. Moreover, eq. S2 in our paper is based on the initial eq. S4:

$$\frac{d^2\varphi}{dx^2} = \frac{2zec_0N_A}{\varepsilon}\sinh\left(\frac{ze\varphi}{kT}\right) \qquad \text{(eq. S4)}$$

It is the linear version, which does not work well with high potentials.[S3] However, it is difficult to solve the answer using full Poisson-Boltzmann equation because of its complex and strict restriction. Therefore, the solution based on a linearized version has been adopted by many researchers.[S4] Here, we use this linear version for the simulation. Although some errors might be existed, the simulation results match with the experimental approach curves.

After applying a voltage of -0.3 and -0.5 V at the electrode, the potential drop in the diffuse layer are achieved and shown in Fig. S3. The signal in SICM comes from the indirect double layer structure rather than the direct Faraday current. As for an electrochemical process, the Faraday current or the consumption of H^+ under -0.5 V brings the additional charge exchange at the electrode. Therefore, this model suits for both non-faradaic and faradic processes.

According to electroneutral theory, the charge of the electrode surface equals to the net charge in the diffuse layer. For a negatively charged electrode, the positive charge is excess. Thus, the charge density can be described as:[S1b]

$$\sigma = \int_0^\infty \left(\sum nc_+ - \sum nc_-\right)Fdx \qquad \text{(eq. S5)}$$

where σ is the charge density at the electrode, F is the Faraday constant, c_- and c_+ are the concentrations of negative and positive ions at a certain distance (x) from the electrode and n is the charge number of corresponding ions (1 for H^+ and HSO_4^-, and 2 for SO_4^{2-}). After the derivation of c_+ and c_- from eq. S1, the charge density under -0.3 and -0.5 V can be achieved from the integral result, as shown in Fig. 2A.

During SICM imaging, most resistance is concentrated at the nanometer sized capillary orifice. According to Ohm's law:

$$I = \frac{U}{R_p + R_t} \qquad \text{(eq. S6)}$$

where I is the current recorded by SICM, U is the bias (e.g. 0.2 V) applied between the inter-capillary electrode and the reference electrode in the solution. Resistance of these two parts are defined as R_p (pipette resistance) and R_t (tip resistance), respectively. According to eq. S6, the approaching curves of I and x under different biases can be obtained and plotted in Fig. 2B.

It is noted that the effect of SICM tip into the steady-state simulation is neglected. Since only ion current flows through the orifice of capillary and no charge is accumulated at the outer wall of the capillary, this presence of the capillary tip might not affect the local charge distribution significantly. A similar simplified simulation is reported by many SICM groups, including Lane Baker[S5] and Patrick Unwin.[S6]

Electric field enhancement based on Laplace equation

In this work, the electric field strength at different regions of an electrode is simulated by Laplace equation. For an electrostatic field, the electric field can be achieved when the space potential is defined:

$$\vec{E} = \nabla\varphi \qquad \text{(eq. S7)}$$

where E is the electric field, φ is the space potential, ∇ is the gradient operator. This equation indicates that the electric field is the gradient of space potential.

To demonstrate the electric field at Pt-graphite surface, a simulation model is developed as shown in Fig. S2. In polar coordinate system, the potential function can be given as:[S7]

$$\varphi = r^n\left[A\cos(n\theta) + B\sin(n\theta)\right] \qquad \text{(eq. S8)}$$

where A, B and n are given constants determined by applied voltage, r is the distance from O point, and θ is the angle as marked in Fig. S2. Electric field can be calculated from eq. S7:

$$E = \left|\vec{E}\right| = \left|-\nabla\varphi\right| = \sqrt{\left(\frac{\partial\varphi}{\partial r}\right)^2 + \left(\frac{1}{r}\frac{\partial\varphi}{\partial\theta}\right)^2} = nr^{n-1}\sqrt{A_n^2 + B_n^2} \qquad \text{(eq. S9)}$$

As A, B and n are the given constants, E is only decided by a factor of r^{n-1}. It is also suitable for three mediums (e.g. Pt, graphite and electrolyte in our work). Then, the question is converted into the value of n, which can be solved from the boundary conditions. For these three mediums, the potential function of three mediums can be given as:

$$\begin{cases} \varphi_1 = r^n\left[A_1\cos(n\theta)+B_1\sin(n\theta)\right] \\ \varphi_2 = r^n\left[A_2\cos(n\theta)+B_2\sin(n\theta)\right] \\ \varphi_3 = r^n\left[A_3\cos(n\theta)+B_3\sin(n\theta)\right] \end{cases} \quad \text{(eq. S10)}$$

And the boundary conditions are listed as follows:

$$\begin{aligned} \theta = 0 &\longrightarrow \left\{ \begin{matrix} \varphi_3 = \varphi_1 \\ \varepsilon_3 \dfrac{\partial \varphi_3}{\partial \theta} = \varepsilon_1 \dfrac{\partial \varphi_1}{\partial \theta} \end{matrix} \right\} \\ \theta = \theta_1 &\longrightarrow \left\{ \begin{matrix} \varphi_1 = \varphi_2 \\ \varepsilon_1 \dfrac{\partial \varphi_1}{\partial \theta} = \varepsilon_2 \dfrac{\partial \varphi_2}{\partial \theta} \end{matrix} \right\} \\ \theta = \theta_2 &\longrightarrow \left\{ \begin{matrix} \varphi_2 = \varphi_3 \\ \varepsilon_2 \dfrac{\partial \varphi_2}{\partial \theta} = \varepsilon_3 \dfrac{\partial \varphi_3}{\partial \theta} \end{matrix} \right\} \\ \theta = 2\pi &\longrightarrow \left\{ \begin{matrix} \varphi_3 = \varphi_1 \\ \varepsilon_3 \dfrac{\partial \varphi_3}{\partial \theta} = \varepsilon_1 \dfrac{\partial \varphi_1}{\partial \theta} \end{matrix} \right\} \end{aligned} \quad \text{(eq. S11)}$$

where ε_1, ε_2 and ε_3 are dielectric constants of the three mediums. Here, medium 1 is platinum (ε_1=6.5), medium 2 is graphite (ε_2=12) and medium 3 is 20 mM H_2SO_4 solution (ε_3=81.5).[S8] To simplify the solving process, the boundary conditions are converted into determinations:

$$\begin{vmatrix} \cos n\theta_1 & \sin n\theta_1 & -\cos n\theta_1 & -\sin n\theta_1 & 0 & 0 \\ \varepsilon_1 \sin n\theta_1 & -\varepsilon_1 \cos n\theta_1 & -\varepsilon_2 \sin n\theta_1 & \varepsilon_2 \cos n\theta_1 & 0 & 0 \\ 0 & 0 & \cos n\theta_2 & \sin n\theta_2 & -\cos n\theta_2 & -\sin n\theta_2 \\ 0 & 0 & \varepsilon_2 \sin n\theta_2 & -\varepsilon_2 \cos n\theta_2 & -\varepsilon_3 \sin n\theta_2 & \varepsilon_3 \cos n\theta_2 \\ -1 & 0 & 0 & 0 & \cos 2n\pi & \sin 2n\pi \\ 0 & \varepsilon_1 & 0 & 0 & \varepsilon_3 \sin 2n\pi & -\varepsilon_3 \cos 2n\pi \end{vmatrix} = 0 \quad \text{(eq. S12)}$$

The determinations can be further simplified combined with actual situation. In the structure of Fig. S4B, the surface of graphite can be considered to be flat. Accordingly, another condition can be adopted that is $\theta_2 = \pi + \theta_1$. The determinations are solved by Matlab:

$$\begin{aligned} &-8(\varepsilon_1\varepsilon_2\varepsilon_3)+(\varepsilon_1+\varepsilon_2)(\varepsilon_2+\varepsilon_3)(\varepsilon_3+\varepsilon_1)\cos 2n\pi \\ &-(\varepsilon_1+\varepsilon_2)(\varepsilon_2-\varepsilon_3)(\varepsilon_3-\varepsilon_1)\cos 2n\theta_1+(\varepsilon_2+\varepsilon_3)(\varepsilon_1-\varepsilon_2)(\varepsilon_3-\varepsilon_1)\cos 2n\theta_1 \\ &+(\varepsilon_1+\varepsilon_3)(\varepsilon_1-\varepsilon_2)(\varepsilon_2-\varepsilon_3)=0 \end{aligned} \quad \text{(eq. S13)}$$

As shown in Fig. S2A, the side of the Pt step is about vertical to graphite substrate. Therefore, θ_1 is set to be 90°. Under this condition, n is ~ 0.7811. Relationship between E and r can be

plotted based on eq. S9. It should be supplemented that from eq. S9, the electric field enhancement scope can extend to millimeters. But in reality, the height of the step is only about 300 nm, the further extension is restrained for the lack of three mediums.

Based on $E = \frac{\varphi}{d}$, electric field strength of infinity is achieved from eq. S2. In eq. S9, it is decided by the constants. As shown in Fig. S3, when -0.3 V is applied to the sample, the effect of the potential extends to ~ 50 nm. For the sample surface, the electric field is ~ 600 kV/cm. For Pt particles at the graphite surface, the similar approach was adopted to research the electric field enhancement. For the areas marked as 1 in Fig. 5C, θ_1 is 45˚ and n is 0.7625. And for the area marked as 2 in Fig. 5C, θ_1 is 45˚ and n is 0.8279.

Fig. S1 X-ray diffraction (XRD) spectrum of Pt layer at the supporting graphite surface.

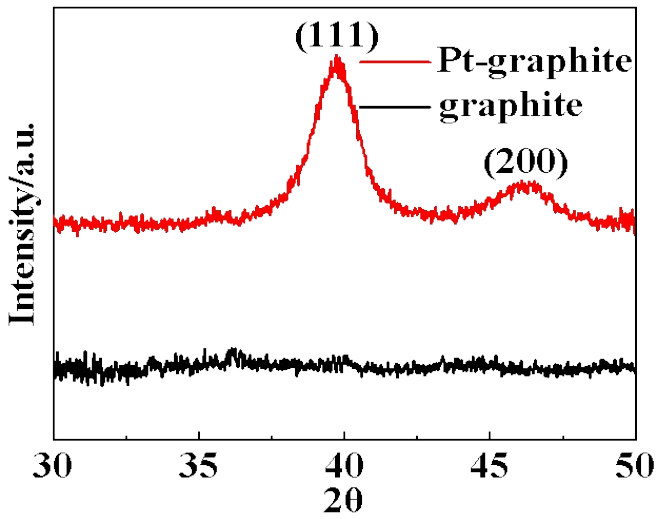

Fig. S2 Schematic of the model based on Laplace equation. (A) supporting graphite; (B) Pt-graphite interface.

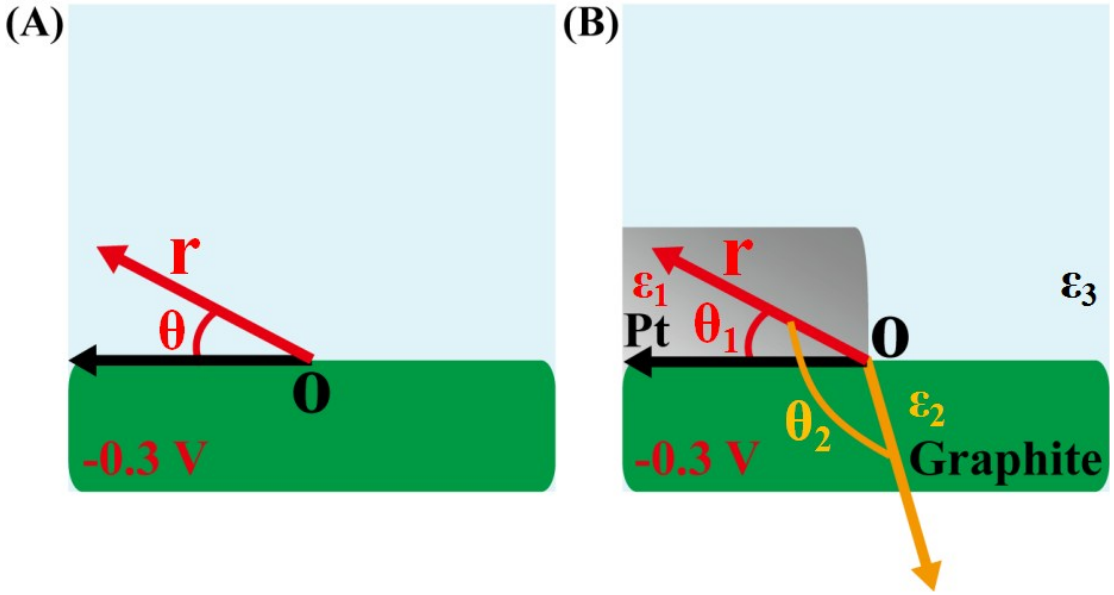

Fig. S3 The simulated potential in the diffuse layer at the Pt-graphite surface.

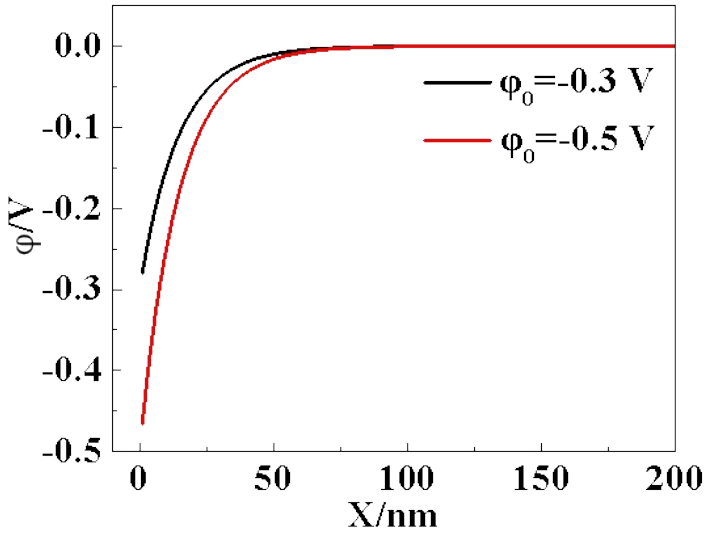

Fig. S4 (A) The reduction currents in 500 mM H_2SO_4 from six randomly selected regions at Pt/grahite interface and planar Pt surface; (B) the charge density at these regions measured in Figure S4A under the potential of -0.3 or -0.5 V. The error bar presents the standard deviation.

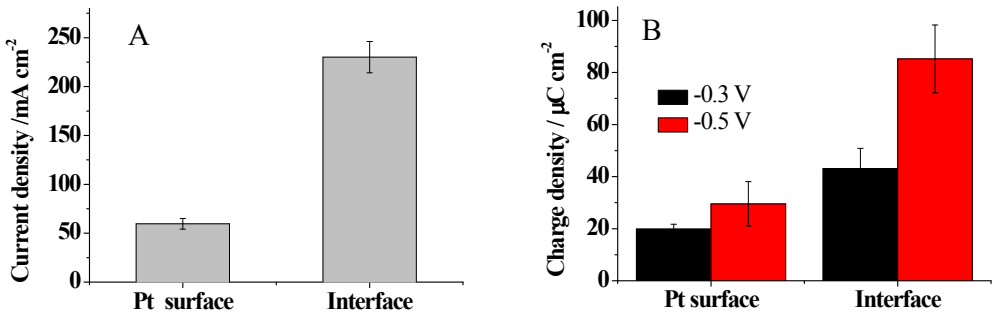

Fig. S5 (A) The Comsol model to calculate the reduction current in 20 mM H_2SO_4 from (i) planar Pt surface and (ii) Pt/graphite interface based on the diffusion module. The region of the electrode is marked in yellow (not to scale). For the planar electrode surface, the size of the electrode is 4 × 10 μm. For the edge electrode at the interface, the height is 0.3 μm, the width is 0.7 μm and the length is 10 μm. The simulation process followed the procedure reported by White group[S9]. (B) The reduction current collected from planar Pt surface (electrode i) and Pt/graphite interface (electrode ii).

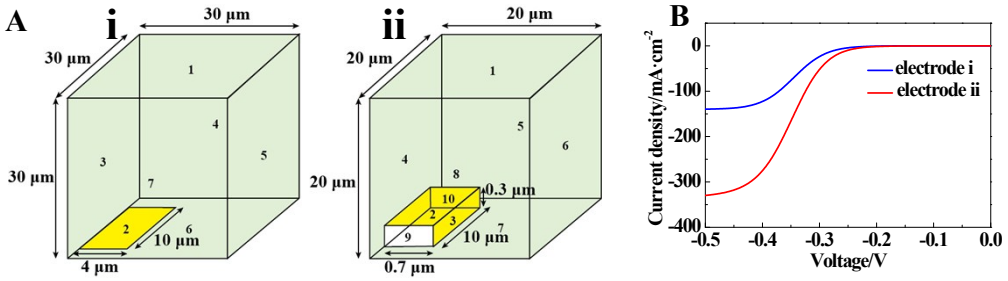

Fig. S6 The schematic setup of in-situ SICM for the characterization of surface charge.

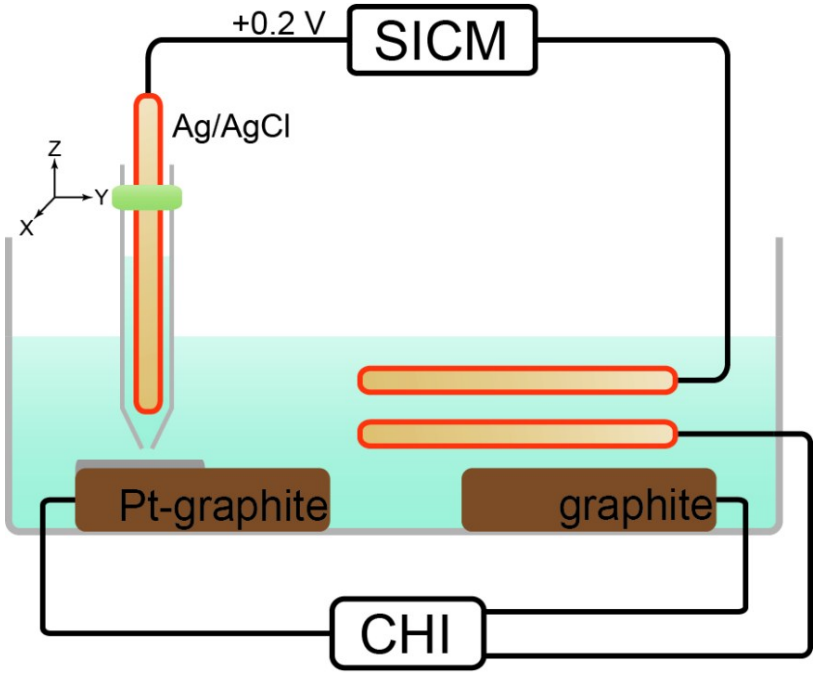

Fig. S7 Current-time curves recorded during the voltage scanning. With a potential of -0.3 V, no electrochemical reduction process occurs. When the potential decreases to -0.5 V, this electro-reduction process starts.

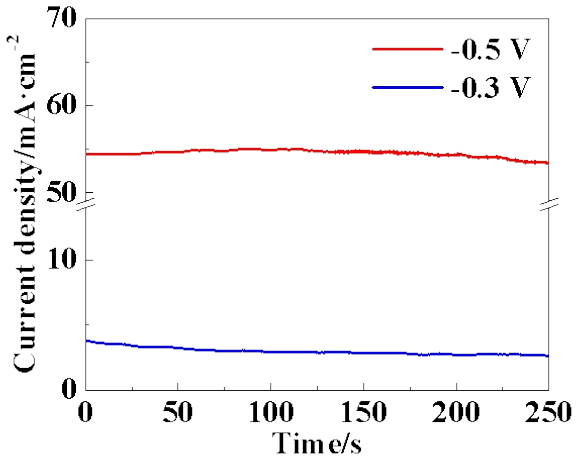

Fig. S8 (A, B) Optical microscope and (C, D) scanning electron microscopic images of the nanocapillary tip before and after the characterization of Pt-graphite surface.

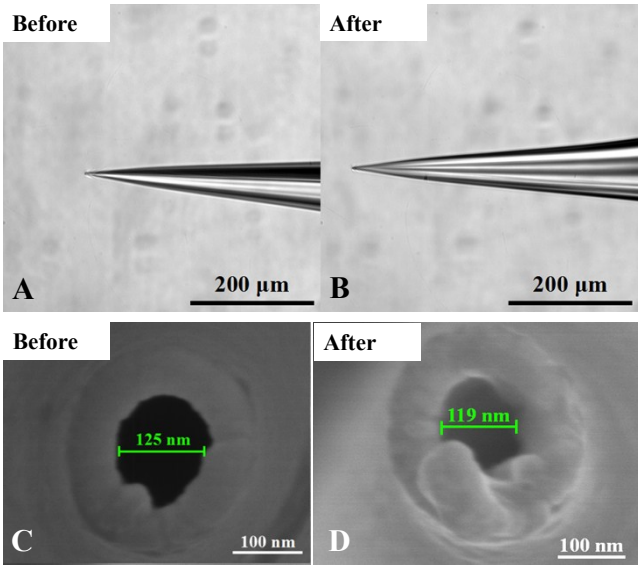

Fig. S9 SICM results of supporting graphite. (A) 2D SICM morphology; (B) 3D (C, D) charge density of graphite with a potential of (C) -0.3 V and (D) -0.5 V.

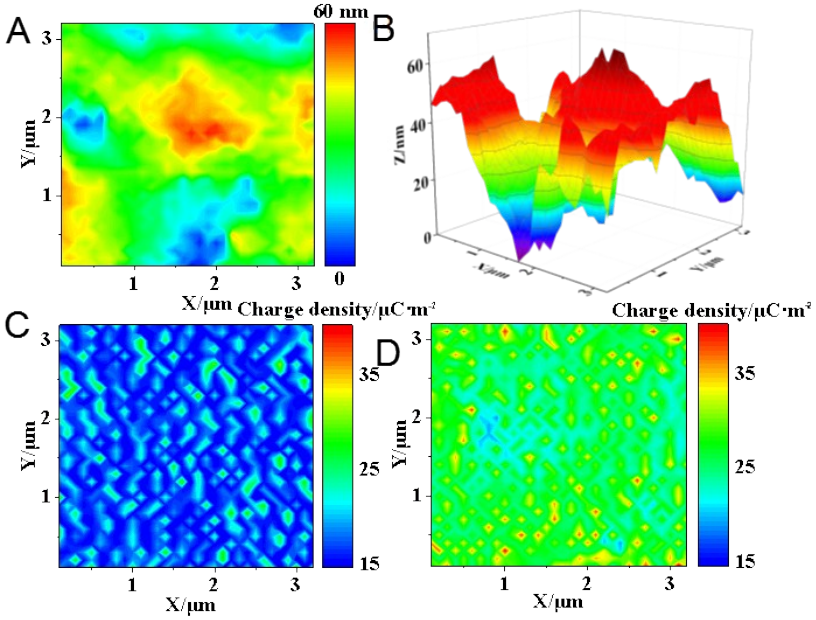

Figure S10. (A) SEM image of TiO_2 layer; (B) SICM image showing the morphology of the Pt-TiO_2 interface; (C) charge density at the Pt-TiO_2 interface at a voltage of -0.5 V; (D) morphology and charge density along the black line in (B) and (C).

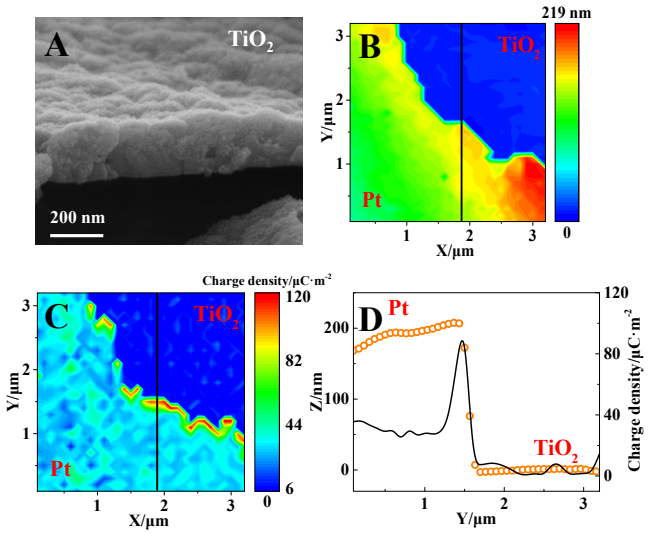

Fig. S11 Element distribution analysis of Pt microparticles at the supporting graphite surface.

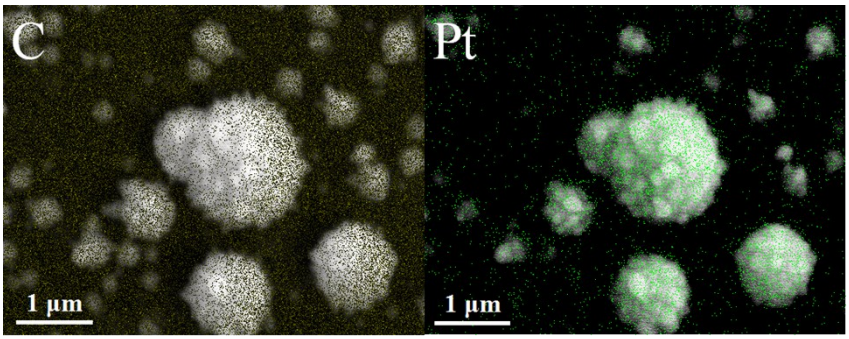

Fig. S12. (A, B) SICM morphology of the two Pt microparticles (A) before and (B) after the application of -0.3 V. (C) the difference in the morphology between (A) and (B).

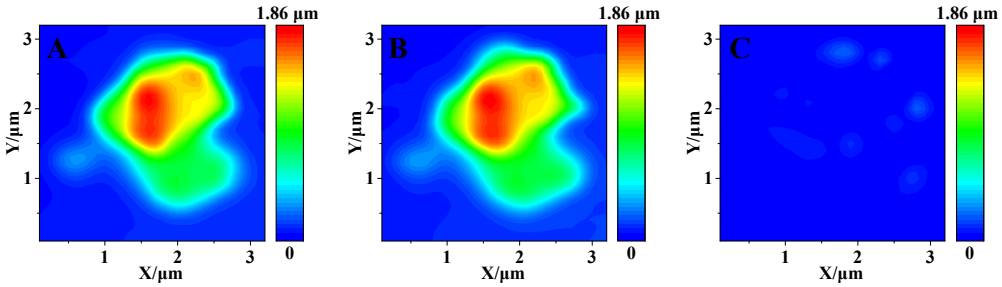

Reference

S1 (a) A. A. Kornyshev, *J. Phys. Chem. B* 2007, **111**, 5545-5557; (b) J. Jiang, D. Cao, D.E. Jiang, J. Wu, *J. Phys.: Condens. Matter* 2014, **26** 284102 (13pp); (c) C. Merlet, C. Pean, B. Rotenberg, P. A. Madden, P. Simon, M. Salanne, *J. Phys. Chem. Lett.* 2013, **4**, 264-268.

S2 J. A. Dean, Lange's Handbook of Chemistry, *Mater. Manuf. Processes* 1990, **5**, 687-688.

S3 E. B. Cummings, S. K. Griffiths, R. H. Nilson, P. H. Paul, *Anal. Chem.* 2000, **72**, 2526-2532.

S4. A. A. Kornyshev, *J. Phys. Chem. B* 2007, **111**, 5545-5557.

S5 (a) D. E. Jiang, J. Wu, *J. Phys. Chem. Lett*. 2013, **4**, 1260-1267; (b) M. O. Bernard, M. Plapp, J. F. Gouyet, *Phys. Rev. E* 2003, **68**, 011604; (c) T. J. Lewis, *J. Phys. D: Appl. Phys*. 2005, **38**, 202-212.

S5 C. C. Chen, L. A. Baker, Analyst 2011, 136, 90-97.

S6 D. Perry, R. A. Botros, D. Momotenko, S. L. Kinnear, P. R. Unwin, *ACS Nano* 2015, **9**, 7266-7276.

S7 A. E. Deprince, R. J. Hinde, Nanoscale Res. Lett. 2010, 5, 592-596.

S8 A. D. Rakic, A. B. Djurisic, J. M. Elazar, M. L. Majewski, *Appl. Opt.* 1998, **37**, 5271-5283.

S9 B. Zhang, Y.H. Zhang, H.S. White, *Anal. Chem.* 2006, **78**, 477-483.